Paper No.
7659

NACE INTERNATIONAL CORROSION 2016 CONFERENCE & EXPO

Effects of CO_2 and H_2S on Corrosion of Martensitic Steels in NaCl at Low Temperature

Ruishu Feng, Justin Beck, Derek M. Hall, Aysel Buyuksagis
and Serguei N. Lvov*
The EMS Energy Institute
Department of Energy and Mineral Engineering
Department of Materials Science and Engineering
The Pennsylvania State University, University Park, PA 16802, USA

Margaret Ziomek-Moroz*
U.S. Department of Energy
National Energy Technology Laboratory
1450 Queen Avenue SW, Albany, OR 97321, USA

*Corresponding authors: lvov@psu.edu
Margaret.Ziomek-Moroz@NETL.DOE.GOV

Corrosion studies were conducted for martensitic carbon steels in brine solutions at 4 °C and 10 MPa (1450 psi), which simulated the subsurface environments encountered in Arctic drilling. Three environments with a 5 % wt. NaCl brine were used: (1) 0.312 mole of CO_2 per mole of H_2O in brine, (2) 3.12 x 10^{-4} mole of H_2S per mole of H_2O in brine, and (3) a mixture of 3.12 x 10^{-4} mole H_2S and 0.312 mole CO_2 per mole of H_2O in brine. Two martensitic carbon steels were selected for the investigations: a high strength low alloy (HSLA) carbon steel commonly used for drill pipe (G41000) and a newly designed ultra-high strength low alloy (UHSLA) steel (G41300). Electrochemical and mass loss measurements found corrosion rates on the order of 0.05 mm y^{-1} in the systems containing H_2S and CO_2+H_2S, while the CO_2 systems saw corrosion rates between 0.5 and 2 mm y^{-1}. Surface analyses of the tested samples were performed using scanning electron microscopy and energy dispersive X-ray spectroscopy to identify corrosion products. The corrosion products were unstable and oxidized quickly after taking out of the system. All samples had a high oxygen content across the surface, though the samples exposed to H_2S and CO_2+H_2S had relatively higher levels of sulfur present in an inner region of the film. Experimental corrosion rates were compared to model predictions, and a good agreement was found for the CO_2 and H_2S cases. However, the model predicted that corrosion rates in the mixed case would match those of the CO_2-only system. The experimental results showed that CO_2:H_2S ratios as high as 1000 can result in predominantly sour corrosion at the low temperature, high pressure conditions tested.

Keywords: H_2S corrosion; CO_2 corrosion; Martensitic carbon steels; Corrosion rate; Corrosion scales; Cold-climate conditions.

©2016 by NACE International.
Requests for permission to publish this manuscript in any form, in part or in whole, must be in writing to
NACE International, Publications Division, 15835 Park Ten Place, Houston, Texas 77084.
The material presented and the views expressed in this paper are solely those of the author(s) and are not necessarily endorsed by the Association.

INTRODUCTION

The presence of CO_2 and H_2S in condensed water phases has for years been of considerable interest to scientists and engineers dealing with corrosion in oil and gas operations, from extraction through processing. One of the major effects of sweet corrosion is that dissolved CO_2 lowers the solution pH and increases the rate of corrosion. Sour corrosion, where H_2S is present, has generally been shown to reduce corrosion rates when low concentrations are present.[1] The mechanism for this drop is the quick formation of a relatively protective iron sulfide film. However, while the reduced material loss may be welcome, the tradeoff of H_2S content is an increased susceptibility for sulfide stress cracking (SSC). With drastically different failure modes being possible, the behavior of mixed systems becomes important for proper design of corrosion prevention and mitigation.

Currently, no widespread law or model exists for determining the transition between sweet and sour corrosion. NACE SP0110 Appendix A describes a rough rule for determining sweet-sour transitions by the CO_2:H_2S ratio based on previous experimental results.[2] A ratio above 500 would be expected to produce predominantly sweet corrosion, while a ratio below 20 would be expected to show predominantly sour corrosion. A ratio between 20 and 500 may allow for a mixed corrosion mechanism where both $FeCO_3$ and FeS could coexist. Work by Smith investigated the assumption of 500 on the upper end of the ratio.[3] Thermodynamic calculations on the stability of $FeCO_3$ and FeS showed that while a ratio of 500 could be justified, it was found to have minor to moderate sensitivity to temperature and ionic strength of the solution and extreme sensitivity to the quality of the thermodynamic data. An example was that a 1 % change in the free energy value for $FeCO_3$ could change the ratio by over a factor of 10.

Another consideration beyond stability of the corrosion products is the understanding of the kinetics for the corrosion process. Work has continued on laboratory experiments investigating the kinetic effects of different CO_2:H_2S ratios over a wide range of conditions. Experiments have shown over a range of conditions CO_2:H_2S ratios from 500 to as high as 10,000 can still see a decrease in corrosion rate by almost an order of magnitude relative to pure CO_2.[4-8] Results at higher H_2S concentrations have ranged between no significant effects to notable increases in corrosion rates, though rates in CO_2-H_2S mixtures were generally lower than in pure CO_2. While a decrease in material loss may be welcome to corrosion engineers, the presence of the more protective iron sulfide films can also make the underlying steels more susceptible to pitting.[9-11] The transition to sour corrosion can also increase the risk of sulfide stress cracking,[12] and the recommendations from ANSI[(1)]/NACE MR0175/ISO[(2)] 15156 should be taken into account.[13]

The purpose of the present work was to provide additional data on corrosion in sweet and sour environments related to oil and gas operations at lower temperatures representative of seafloor or Arctic operations. The tests investigated corrosion in brines at equilibrium with CO_2, H_2S, and a mixed phase at a CO_2:H_2S ratio of 1000 at 4 °C and 10 MPa total pressure using electrochemical techniques, mass loss measurements, software modeling, and surface analyses.

EXPERIMENTAL

Test Conditions

The goal of the study was to investigate an environment representative of low temperature Arctic drilling conditions. A temperature of 4 °C was selected with a total system pressure of 10 MPa. A 5 % wt. NaCl (0.9 mol kg^{-1}) brine was selected for the test solution. The sweet/sour/mixed conditions were prepared by holding the test solution in equilibrium with one of three secondary phases: pure CO_2, an H_2S/Ar mixture, and a CO_2/H_2S/Ar mixture. It should be noted that the target test conditions were above the CO_2 critical pressure (7.39 MPa) but below the CO_2 critical temperature (31 °C), and it was above both the

(1) American National Standards Institute (ANSI), 1899 L Street, NW, 11th Floor, Washington, DC, 20036
(2) International Organization for Standardization (ISO), Chemin de Blandonnet 8, CP401, 1214 Vernier, Geneva, Switzerland

©2016 by NACE International.
Requests for permission to publish this manuscript in any form, in part or in whole, must be in writing to
NACE International, Publications Division, 15835 Park Ten Place, Houston, Texas 77084.
The material presented and the views expressed in this paper are solely those of the author(s) and are not necessarily endorsed by the Association.

critical pressure (4.863 MPa) and critical temperature (-122.5 °C) of Ar. Care should be taken at high pressures when referring to such substances as “gas” or “vapor” phases, and describing their concentrations in terms of partial pressures may not accurately reflect their composition in the system.

Taking this into account, the conditions and test procedure were designed to allow consistent dosing of substances while maintaining concentrations representative of deep-well environments. The goal was to simulate downhole environments predicted for deep oil and gas wells.[14] Deep wells are predicted to encounter total pressures up to and above 100 MPa, and the “gas” phase may contain over 10 % CO_2 and 0.01 % H_2S. A simplified assumption was employed for this study. The tests systems were initially calculated to represent exposure to a pocket of CO_2- and/or H_2S-containing secondary phase (either gas or condensed phase) with 10 MPa of CO_2 and/or 0.01 MPa of H_2S. A 1:1 ratio of aqueous:non-aqueous volume was considered as coming to equilibrium; this allowed a calculation of the total contents (in moles) of each component (water, NaCl, CO_2, and H_2S) in the total system. Thus, the entire system could be defined as a mole X:mole water ratio, where X represents any non-water species in the system.

The initial calculation results had to be adapted to account for physical limitations in the system when maintaining the proper mole ratios, particularly maintaining a safe amount of non-aqueous phase at the top of the autoclave vessel to prevent severe pressure increases if cooling was lost to the system. The final ratios used for these tests was 0.312 mole CO_2:mole H_2O and 3.12 x 10^{-4} mole H_2S:mole H_2O (maintaining a CO_2:H_2S = 1000:1 ratio for the mixed case). The Ar:H_2O ratio was not controlled, but rather argon was used to dilute the H_2S and balance the pressure between tests. Phase equilibria calculations were performed using commercial thermodynamic modeling software to determine the final amounts of each species needed to achieve the internal autoclave volume (476 mL assembled) at 4 °C and a total pressure of 10 MPa.

Materials Investigated

Two high-strength low alloy martensitic drilling steels were tested. The first was a high strength low alloy (HSLA) steel (G41000), while the second was an ultra-high strength low alloy (UHSLA) steel (G41300) with a higher strength. Chemical compositions for each tested alloy are given in Table 1. The primary differences in composition were lower chromium and higher manganese, nickel, copper, and vanadium in the UHSLA versus the HSLA. The level of sulfur was also higher for the UHSLA. The result is an alloy with an 8 % higher yield strength and a 9 % higher ultimate tensile strength, as seen in Table 2.[15]

Table 1. Chemical compositions (mass%) of UHSLA and HSLA[15]

Grade	Fe	Cr	Mn	Mo	Al	Ni	Cu	Nb	S
UHSLA	Bal	0.79	0.88	0.67	0.03	0.81	0.19	0.02	0.007
HSLA	Bal	1.39	0.78	0.68	0.03	0.02	0.02	<0.01	0.002

Grade	P	B	C	N	V	Si	Sn	Tl
UHSLA	<0.005	<0.005	0.27	0.007	0.07	0.26	<0.01	0.07
HSLA	0.006	<0.005	0.26	0.005	<0.01	0.3	<0.01	<0.01

Table 2. Mechanical properties of UHSLA and HSLA

Grade	Yield strength, MPa	Ultimate tensile stress, MPa
UHSLA	1183	1278
HSLA	1096	1168

Electrodes for the electrochemical tests were prepared using 10x10x5 mm plates. One 10x10 mm face served as the electrode surface, and a 304 stainless steel (UNS S30400) electrode lead was attached to the opposite face. The electrode lead was coated with shrinkable polytetrafluoroethylene (PTFE) tubing. Two to three electrode plates were placed into a PTFE holder and all sides other than the 10x10 mm electrode surface were sealed to the PTFE using a high temperature epoxy. Mass loss samples were also prepared using 25x20x2 mm plates. A 3 mm ID hole was drilled near the top of the plate so that the samples could be suspended from a PTFE-coated wire. The electrode surface and mass loss sample

©2016 by NACE International.
Requests for permission to publish this manuscript in any form, in part or in whole, must be in writing to
NACE International, Publications Division, 15835 Park Ten Place, Houston, Texas 77084.
The material presented and the views expressed in this paper are solely those of the author(s) and are not necessarily endorsed by the Association.

were each polished with 600 grit SiC paper and then cleaned for 30 to 60 minutes in acetone in a sonic bath.

System Setup

The electrochemical measurements were performed using a three electrode system. The working electrodes consisted of two to three of the steel samples prepared as described above. The counter electrodes were 20x10 mm sheets of either platinum plate or mesh. The electrode leads were coated with PTFE. Two to three of these counter electrodes were inserted through the edges of the PTFE working electrode assembly to allow each to be placed parallel to a working electrode in the system. An example of the completed assembly is shown in Figure 1. Two mass loss samples were suspended by PTFE-coated wire from the autoclave lid, with care taken to ensure that they would remain in the aqueous phase without contacting any of the inner surfaces.

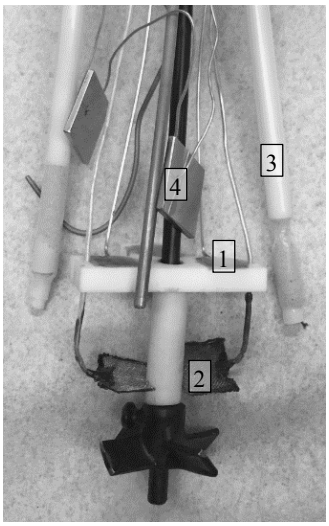

Figure 1. Electrode assembly for autoclave tests (1-Working electrode, 2-Counter electrode, 3-Reference electrode, 4-Mass loss sample).

Custom double-junction silver-silver chloride electrodes were prepared for the high pressure systems. The reference solution was 5 % wt. NaCl to reduce the effects of liquid junctions on the electrode potential. The inner junction of the reference electrodes consisted of solution-saturated zirconia sand sealed with the Ag/AgCl electrode inside an alumina tube with high temperature epoxy. The inner junction was prepared using a porous zirconia-magnesia cement. The second junction was prepared by sealing a shrinkable PTFE tube around the outside of the ceramic tube. The inside of the PTFE tube was filled again with solution-saturated sand, and either another cement frit or a perforated PTFE plug was used for the second junction. Two reference electrodes were used for each test in case one failed before the end of the exposure, and new electrodes were prepared for each assembled autoclave. Further details can be found in Reference 16. The potential of the Ag/AgCl electrode in 5 % wt. NaCl at 4 °C was calculated to be 0.2497 V vs. the standard hydrogen electrode (SHE) using the commercial modeling software. The results were confirmed through comparison to calculations performed using thermodynamic properties and activity coefficients from literature.[17,18]

All measurements were performed in a 600 mL autoclave vessel. A PTFE liner was used to isolate the test solution from the autoclave vessel. Temperature was controlled using a circulating chiller and a copper-coil heat exchanger wrapped around the autoclave vessel. All tests were stirred using an impeller rotating at around 150 rpm. A computer-controlled potentiostat was used to perform the electrochemical measurements, which included linear polarization resistance (LPR), electrochemical impedance spectroscopy (EIS), and cyclic voltammetry (CV).

©2016 by NACE International.
Requests for permission to publish this manuscript in any form, in part or in whole, must be in writing to
NACE International, Publications Division, 15835 Park Ten Place, Houston, Texas 77084.
The material presented and the views expressed in this paper are solely those of the author(s) and are not necessarily endorsed by the Association.

Experimental Procedure

The autoclave contents, in moles, for each of the three test environments are given in Table 3. The addition of materials was generally as follows due to requirements related to achieving 10 MPa final system pressure. First, the autoclave was assembled dry with all electrodes and mass loss samples. Only one alloy (either HSLA or UHSLA) was present in each assembled autoclave. The desired amount of NaCl(s) was placed at the bottom of the vessel before it was sealed. The sealed vessel was then purged of oxygen by repeated and slow pressurization and depressurization cycles up to 20 bar (300 psi). Care had to be taken to prevent gas bubbles from forming at the reference electrode junctions. This was believed to have caused failure of some of the electrodes during exposure. During this process the cooling was started to bring the system down to 4 °C. This usually involved letting the system chill overnight to ensure it was at a stable temperature for H_2S injection. The temperature stability was typically within ±1 °C, though on hot days the variability could be as high as ±3 °C.

After the autoclave was deaerated, the system was brought down to just above atmospheric pressure (to maintain positive pressurization) and H_2S was added (if needed) using a 10 %vol. H_2S in Ar blend. The desired pressure was calculated using the autoclave volume (476 mL after assembly) and the ideal gas law at 4 °C. In the H_2S-only tests, the H_2S addition was followed by further addition of argon to help balance the final pressure. The water injection was performed using deaerated deionized water (deaerated with Ar for > 1 hour) and a high performance liquid chromatography (HPLC) pump. The HPLC pump was set to a constant flow rate of 10 mL min^{-1} and run until the desired amount of water had been transferred to the system. For the H_2S-only tests, water injection was the final step and was used to bring the test system to its final pressure. It should be noted that while the target pressure was 10 MPa, the actual pressure was in the range of 6 to 8 MPa due to small errors in water addition and determining the internal autoclave volume. These errors were magnified due to the small non-aqueous volume relative to the incompressible aqueous phase. For the CO_2 and CO_2+H_2S tests CO_2 was added as the final step to bring the system up to 10 MPa. CO_2 was added using a supercritical CO_2 pump which was a modified design of the HPLC pump used for water injection. Additional CO_2 had to be added over the first 12 hours to account for pressure drops due to the dissolution of CO_2 into the aqueous solution.

TABLE 3. Test conditions for corrosion exposure

Gas	T /°C	P /MPa	V /mL	H_2S /mole	CO_2 /mole	H_2O /mole	NaCl /mole	Ar /mole
CO_2	4	10	476	0	4.52	14.49	0.2350	0
CO_2+H_2S	4	10	476	4.493×10^{-3}	4.493	14.40	0.2334	4.044×10^{-2}
H_2S	4	10	476	6.302×10^{-3}	0	20.20	0.32746	0.5597

After all components were added the autoclave was sealed for the remainder of the exposure period. LPR and EIS measurements were performed regularly for at least 60 hours until the system approached steady-state behavior. LPR was measured at 0.01 mV s^{-1} over a range of ±15 mV around the corrosion potential E_{corr}. EIS was performed with an amplitude 10 mV over a frequency range from 300 kHz down to 5 mHz. After the system reached steady state, cyclic voltammetry sweeps were run at sweep rates of 100, 50, and 5 mV s^{-1}. One electrode was not polarized with CV and was used for surface analysis. Total exposure time ranged from 90 to 120 hours and was recorded for mass loss calculations.

After the electrochemical tests were completed the autoclave systems were depressurized and disassembled. All electrodes and mass loss samples were rinsed with distilled water, dried with argon, and sealed in sample bags under argon. One electrode for each alloy from each condition was used for surface analysis using scanning electron microscopy (SEM) and energy dispersive X-ray spectroscopy (EDS). Mass loss samples were cleaned and analyzed according to ASTM[(3)] G1 using Solution C.3.5 (HCl and hexamethylene tetramine) from Appendix A1.[19] Freshly polished, unexposed samples for each alloy were cleaned to serve as calibrations and account for material loss due to the cleaning procedure.

[(3)] ASTM International, 100 Barr Harbor Drive, PO Box C700, West Conshohocken, PA, 19428

©2016 by NACE International.
Requests for permission to publish this manuscript in any form, in part or in whole, must be in writing to
NACE International, Publications Division, 15835 Park Ten Place, Houston, Texas 77084.
The material presented and the views expressed in this paper are solely those of the author(s) and are not necessarily endorsed by the Association.

RESULTS AND DISCUSSION

Corrosion Results from LPR, EIS, and Mass Loss

Both alloys showed an obvious correlation between the corrosion rate (CR) and the presence of H_2S. The average results for at least two samples at each condition are given in Table 4 along with the standard deviation. The polarization resistance, R_{pol}, from both LPR and EIS increased by more than one order of magnitude when H_2S was added, corresponding to a one order of magnitude drop in corrosion rate. A small increase in corrosion rate was observed when CO_2 was removed from the environment, though this difference almost negligible when compared to the CO_2-only corrosion rates. This matched behavior that has been reported for low concentrations of H_2S, both with and without CO_2 in a wide range of laboratory studies. It can be seen that in the low temperature, high pressure environment tested here a CO_2:H_2S ratio as high as 1000 was still enough to transition from sweet to sour corrosion. While a decrease in material loss is generally welcome in corroding systems, the tradeoff for the protection of iron sulfide can be an increased risk for cracking. For this reason, laboratory corrosion measurements for sour corrosion should be coupled with mechanical testing where possible to determine if the decrease in corrosion rate from the transition from sweet to sour corrosion coincides with increased susceptibility to sulfide stress cracking.

TABLE 4. Corrosion results for HSLA and UHSLA

		LPR		EIS		Mass Loss	Modeled
Alloy	Gas	R_{pol}, Ω cm^2	CR, mm y^{-1}	R_{pol}, Ω cm^2	CR, mm y^{-1}	CR, mm y^{-1}	CR, mm y^{-1}
HSLA	CO_2	336±59	0.418±0.074	326±46	0.429±0.061	0.590±0.019	2.19
	CO_2+H_2S	8067±3048	0.0189±0.0070	8236±3213	0.0187±0.0080	0.0599±0.0147	2.36
	H_2S	4038±483	0.0346±0.0042	4013±566	0.0350±0.0050	0.0798±0.0143	0.0419
UHSLA	CO_2	76.42±6.58	1.82±0.16	94.9±17.6	1.49±0.27	1.77±0.32	2.21
	CO_2+H_2S	4180±526	0.0334±0.0042	4286±711	0.0328±0.0054	0.0877±0.0043	2.38
	H_2S	2722±184	0.0510±0.0036	2702±206	0.0515±0.0041	0.0678±0.024	0.0593

Very good agreement was seen between the LPR and EIS results. Good agreement was seen between the corrosion rates from the electrochemical and mass loss measurements in the CO_2-only environment. However, the disagreement was greater when H_2S was present, where corrosion rates from mass loss were consistently larger than those from the electrochemical tests. The difference was attributed to errors in the mass loss measurements due to the lower corrosion rates. It was found that the material lost from each exposure to cleaning solution was of a similar order to the mass lost from corrosion, which likely resulted in an exaggerated corrosion rate. In all three environments the UHSLA alloy gave a higher overall corrosion rate than HSLA for the electrochemical tests, even after accounting for the standard deviation between samples. The difference was roughly a factor of two in the presence of H_2S, but was as much as four times larger in the CO_2-only system. The trend was not present in the mass loss data for the H_2S-containing systems but was seen in the CO_2-only system. This may again have been due to measurement error in the mass loss samples.

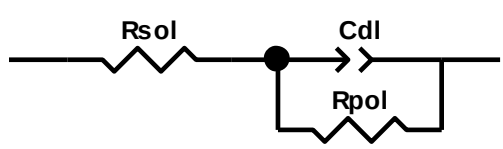

Figure 2. Equivalent circuit used to fit EIS data.

©2016 by NACE International.
Requests for permission to publish this manuscript in any form, in part or in whole, must be in writing to
NACE International, Publications Division, 15835 Park Ten Place, Houston, Texas 77084.
The material presented and the views expressed in this paper are solely those of the author(s) and are not necessarily endorsed by the Association.

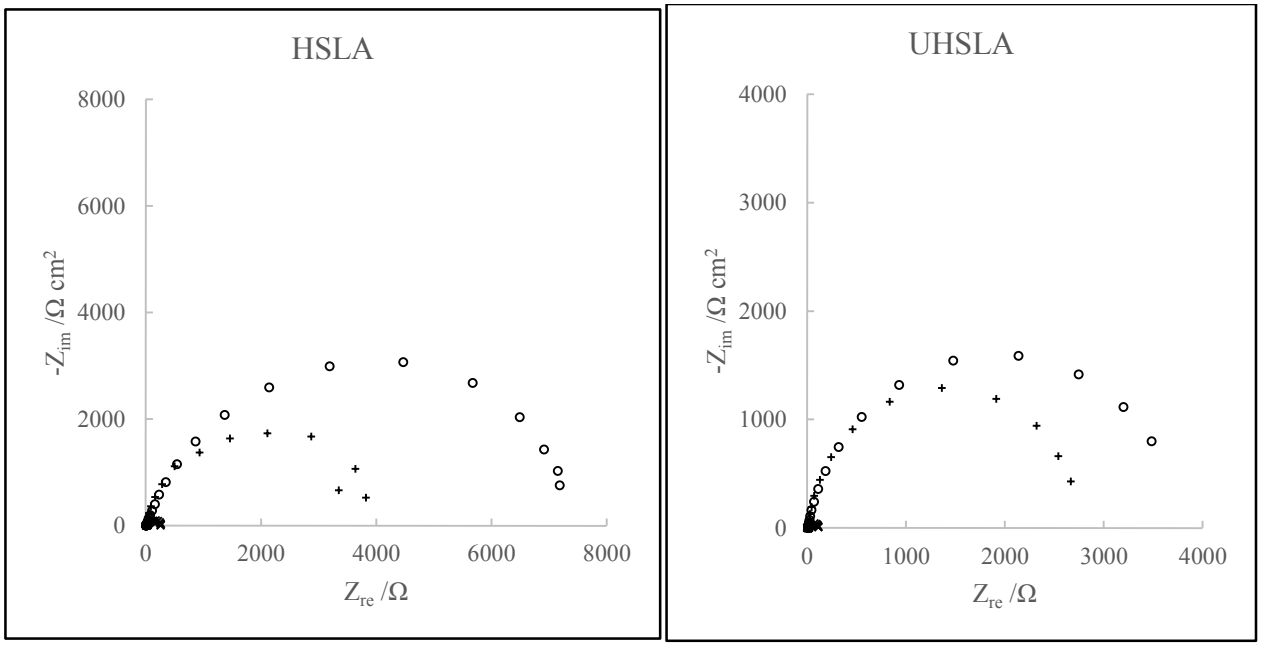

Figure 3. Nyquist plots for HSLA (left) and UHSLA (right). Conditions: 4 ºC, 0.9 mol kg^{-1} NaCl. 10 MPa; x = CO_2, o = CO_2+H_2S, + = H_2S.

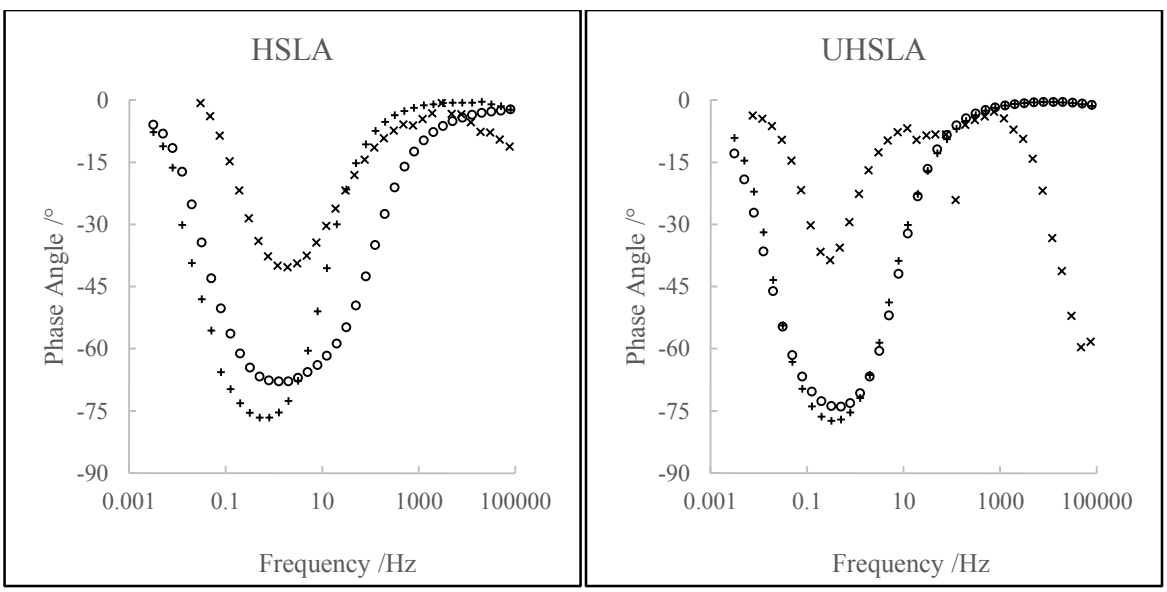

Figure 4. Bode phase angle plots for HSLA (left) and UHSLA (right). Conditions: 4 ºC, 0.9 mol kg^{-1} NaCl. 10 MPa; x = CO_2, o = CO_2+H_2S, + = H_2S.

The corrosion rates were calculated assuming activation-controlled corrosion behavior, which was confirmed in the EIS results. The data was fit using the Randles circuit without diffusion shown in Figure 2. R_{sol} represents the solution resistance, and R_{pol} represents the polarization resistance. A constant phase element (CPE) was used to account for non-ideality of the double layer capacitance. As shown in Figures 3 and 4, only one time constant was observed in all three environments. Small inductive- or capacitive-type behaviors were seen at frequencies above 10^5 Hz, though no correlations were determined between these time constants and the corrosion behavior. One exception was the UHSLA samples in the CO_2 system, where the higher frequency capacitive behavior extended down to around 10^3 Hz. The total impedances at the upper frequencies were small compared to the maximum impedance, which could explain why they were not found to affect the overall corrosion behavior. In addition to the

©2016 by NACE International.
Requests for permission to publish this manuscript in any form, in part or in whole, must be in writing to
NACE International, Publications Division, 15835 Park Ten Place, Houston, Texas 77084.
The material presented and the views expressed in this paper are solely those of the author(s) and are not necessarily endorsed by the Association.

dramatic increase in impedance in the presence of H_2S, it can be seen in the phase angle plots in Figure 4 that the transition to sour corrosion doubled the maximum phase angle, suggesting that the double layer capacitance in sour environments was more ideal than that in the CO_2-only systems. There was no significant or consistent shift in the frequency at which this peak was observed, suggesting that the overall capacitance of the corrosion product film did not change greatly with the change in corrosion rate. An increase in capacitance would be expected to require a longer polarization for the total charge to be filled, which would then shift the phase angle peak to a lower frequency.

Cyclic Voltammetry

The CV curves for the two tested alloys are shown in Figure 5. All curves were corrected to take into account the solution resistance determined from EIS. Two distinct trends were observed. First and foremost, a consistent peak was seen in the anodic sweep for both alloys in the H_2S and CO_2+H_2S systems that was absent in the CO_2-only system. It is believed that this peak thus corresponded to a sulfide-related process. This peak was within about 100 mV of the measured E_{corr} in each case, meaning that the process was likely present as part of the corrosion process. The second trend was that the anodic slope for the H_2S and CO_2+H_2S curves notably steeper than for the CO_2 curve, suggesting that for both alloys the presence of H_2S was affecting the corrosion mechanism and not just reducing the available reactive area. Trends for the cathodic side of the sweep were inconsistent and no similar conclusions were drawn. Sweeps at 100 mV s^{-1} showed nearly identical behavior to those shown in Figure 5 at 50 mV s^{-1}, only with larger currents. In sweeps at 10 mV s^{-1} the magnitude of the H_2S-related peak was much smaller than at 50 mV s^{-1} and in some cases was difficult to distinguish.

Corrosion Modeling Results

The experimental results were compared to those calculated for each condition using commercial modeling software,[20,21] and the modeled CR results are given in Table 4. Calculations were performed assuming a generic carbon steel. The inputs for the test environments were those listed in Table 3. Hydrodynamic effects were approximated as a 10 mm OD rotating disk electrode at 150 rpm, though hydrodynamic effects were found to have only a minor impact on the calculations at the test conditions. The solution pH was predicted to be around 2.86 for both environments containing CO_2 and 4.45 for the H_2S-only environment. This corresponds to the lower concentration of acid gas in the H_2S-only case.

The results of the corrosion modeling in the CO_2 environment were found to be quite good for UHSLA, and though the experimental value for HSLA was significantly lower it was still within a reasonable range. Similar agreement was seen in the H_2S environment as well. The results for UHSLA were very close to the modeled values, and the results for HSLA were within a factor of two. Overall, the model for these conditions was considered quite good when considering that a general carbon steel was assumed in place of the specific alloys tested. Substantial disagreement was seen in the CO_2+H_2S mixture. The experimental results found that the mixed case behaved very close to the H_2S-only condition, indicating sour corrosion was dominant. However, the modeled results were quite similar to sweet corrosion, resulting in overly high predictions of corrosion rates. Increasing the amount of H_2S in the model, thereby decreasing the CO_2:H_2S ratio, only increased the predicted corrosion rate, showing that the issue was not a simple “tipping point” between sweet and sour corrosion. Decreasing the amount of CO_2 in the model (while keeping H_2S constant) decreased the predicted corrosion rate but did not reach the low rates of the H_2S-only case.

©2016 by NACE International.
Requests for permission to publish this manuscript in any form, in part or in whole, must be in writing to
NACE International, Publications Division, 15835 Park Ten Place, Houston, Texas 77084.
The material presented and the views expressed in this paper are solely those of the author(s) and are not necessarily endorsed by the Association.

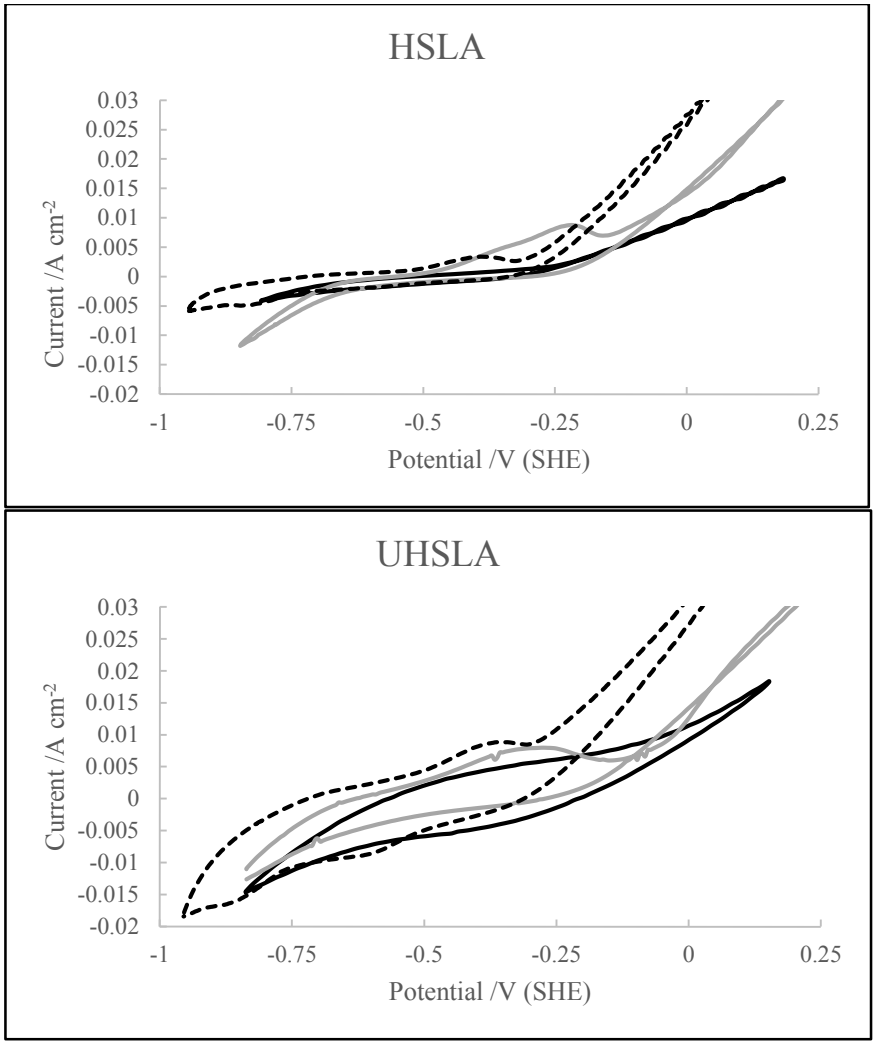

Figure 5. Cyclic voltammetry curves for HSLA (top) and UHSLA (bottom) at 50 mV s^{-1}. Conditions: 4 ºC, 0.9 mol kg^{-1} NaCl. 10 MPa; black = CO_2, grey = CO_2+H_2S, dashed = H_2S.

TABLE 5. Experimental and modeled corrosion potentials

Gas	HSLA /V (SHE)	UHSLA /V (SHE)	Modeled /V (SHE)
CO_2	-0.353±0.001	-0.332±0.001	-0.374
CO_2+H_2S	-0.337±0.004	-0.337±0.004	-0.376
H_2S	-0.444±0.002	-0.460±0.002	-0.463

Table 5 shows comparisons of the measured E_{corr} and those calculated using the modeling software. The standard deviation at each condition is also included. It can be seen that, unlike the corrosion rate, E_{corr} was strongly correlated with the presence of CO_2 rather than H_2S. This suggested that the corrosion potential was more a function of pH, which was predicted to be 2.86 for the systems containing CO2 and 4.46 for the system without. This would affect the equilibrium potential for the cathodic reaction, which could in turn shift the corrosion potential to a more positive value when the pH is lower. It could also affect the equilibrium potential for the anodic reaction by changing the solubility of corrosion products in the aqueous phase. The modeled values for all conditions were in good agreement with the experimental data. Importantly, the model correctly predicted the change in E_{corr} when CO_2 was not present in the system.

©2016 by NACE International.
Requests for permission to publish this manuscript in any form, in part or in whole, must be in writing to
NACE International, Publications Division, 15835 Park Ten Place, Houston, Texas 77084.
The material presented and the views expressed in this paper are solely those of the author(s) and are not necessarily endorsed by the Association.

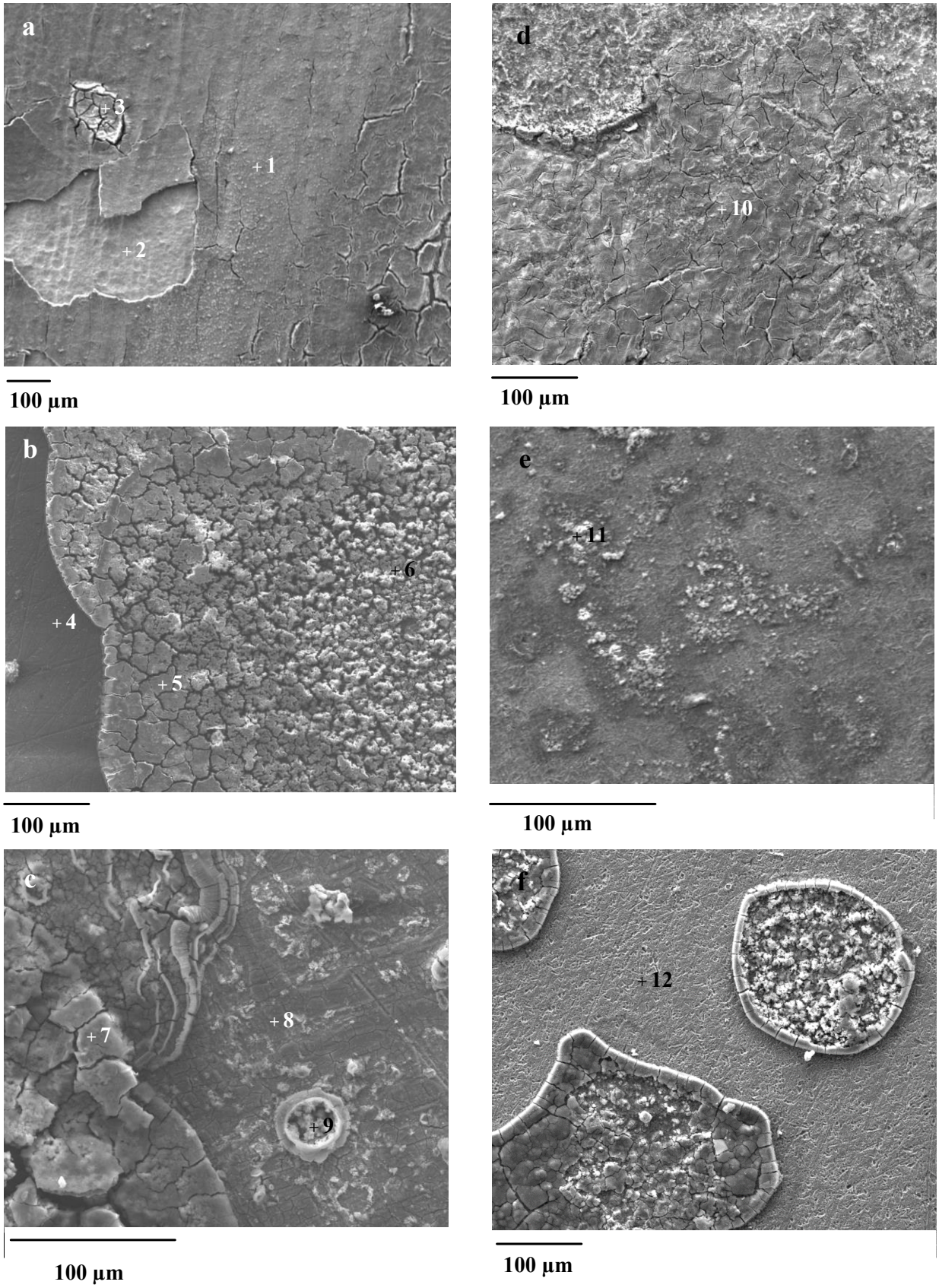

Figure 6. SEM images of the corroded UHSLA (a,b,c) and HSLA (d,e,f) steel surfaces. Conditions: 4 ºC, 0.9 mol kg^{-1} NaCl. 10 MPa, a,d: CO_2; b,e: CO_2+H_2S; c,f: H_2S.

©2016 by NACE International.
Requests for permission to publish this manuscript in any form, in part or in whole, must be in writing to
NACE International, Publications Division, 15835 Park Ten Place, Houston, Texas 77084.
The material presented and the views expressed in this paper are solely those of the author(s) and are not necessarily endorsed by the Association.

Surface Analysis

In all the three conditions, the corrosion scale on the sample surface changed from black to orange quickly during rinsing with distilled water and drying with argon after taking the samples out of the autoclave. A large amount of oxygen was detected using EDS on the surface for both UHSLA and HSLA. Due to the discoloration on rinsing, it was believed that a significant portion of the oxygen present on the sample surface may have been due to oxidation of the existing corrosion product to hematite after the system was disassembled. This showed that the stability of the corrosion product film was quite conditional, and well upsets where the oxygen content of the downhole solution increases could result in a breakdown of the corrosion film.

Figure 6 shows SEM images of the corroded steel surfaces and the EDS analysis results on the selected locations are listed in Table 6. The accelerating voltage was 10 kV. In the pure CO_2 condition for UHSLA, the steel surface was covered with corrosion scales of high oxygen content. The Fe:O ratio was close to 1:2. The scales cracked and stripped off from the surface in some regions, and the steel surface was exposed. In the CO_2+H_2S condition, two regions were observed on the corroded surface of UHSLA: a thick product layer region with a composition close to 2Fe:3O, and a thin product film region containing lower O and relatively higher S as in Location 4. In the pure H_2S condition, the chemical composition over the surface was close to 1Fe:2O and 2Fe:3O. It could have been that FeO(OH) or Fe_2O_3 formed after drying the sample, as goethite, hydrohematite, or hematite could all give the reddish color observed after rinsing.[22] S was relatively higher in the thin layer region (2.5%~6%at), while O was dominant across the surface. Generally, the morphology had two distinct regions with the presence of H_2S, and relatively higher S was found in the thin layer region. As this region correlated with a considerable drop in corrosion rate for the H_2S-containing systems, it was considered that the S-containing scale had a protective effect.

TABLE 6. EDS chemical analyses in at.% on the corroded surfaces in selected locations marked in Figure 6.

Steel	Location	Fe	C	O	S	Na	Cl
UHSLA	1	26	8	63	-	0.3	0.4
	2	78	13	6.6	-	0.3	0.1
	3	29	8.4	56	-	0.1	1.6
	4	56	-	28	4.5	0.8	0.2
	5	34	-	63	0.1	0.2	2.4
	6	37	-	58	0.2	0.1	4.3
	7	34	3.1	59	0.4	0.3	2.5
	8	27	13	51	5.9	1.2	0.8
	9	34	5.9	55	0.5	0.3	3.8
HSLA	10	33	16	47	-	0.1	0.1
	11	38	-	60	0.7	-	1.0
	12	56	16	26	1.1	-	0.3

HSLA showed the similar trend of chemical compositions in the three different conditions like UHSLA. However, subtle difference in surface morphology were observed. In many cases, surface features present on both alloys were found to be smaller on the HSLA samples. On both alloys, particularly for the H_2S-containing systems, pockets of high-O corrosion product tended to be round and appeared similar in shape to water droplets. This could be evidence that the highly-oxidized features occurred after the system was disassembled, and that the lower-O regions may be more representative of the surface at test conditions.

CONCLUSIONS

Experimental results for two drilling steels, HSLA and UHSLA, showed a distinct drop in corrosion rate when transitioning from sweet to sour corrosion in 5% wt. NaCl brine at at 4 °C and 10 MPa total pressure. It was found that a CO_2:H_2S ratio as high as 1000 was still enough for sour corrosion to dominate the conditions tested. H_2S and CO_2+H_2S environments gave corrosion rates on order of 0.05

©2016 by NACE International.
Requests for permission to publish this manuscript in any form, in part or in whole, must be in writing to
NACE International, Publications Division, 15835 Park Ten Place, Houston, Texas 77084.
The material presented and the views expressed in this paper are solely those of the author(s) and are not necessarily endorsed by the Association.

mm y^{-1}, whereas corrosion in the CO_2 environment was on the order of 0.5 to 2 mm y^{-1}. CV sweeps found a current peak within 100 mV of E_{corr} for all samples in the H_2S and CO_2+H_2S systems, which was believed to correlate to a sulfide-related process in the anodic reaction. Further, anodic slopes at larger polarizations were higher than those in the CO_2-only environment.

Comparisons were made between the experimental results and those from a commercial software model. Good agreement was seen in the CO_2 and H_2S conditions. However, the model predicted that corrosion in the mixed CO_2+H_2S system would match that of CO_2, whereas experimental results found that it matched those from the H_2S system. In all cases the model was found to provide a good prediction for E_{corr}. Corrosion potentials in the CO_2 and CO_2+H_2S systems were almost identical, while a roughly 100 mV decrease was seen in the H_2S system. This suggested that while the corrosion behavior was strongly dependent on the H_2S content, the corrosion potential was instead tied to the CO_2 content of the system.

The corrosion products for all tests were found to be quickly oxidized on exposure to air when the system was disassembled. All samples showed high oxygen content across the surface, while the samples exposed to H_2S and CO_2+H_2S appeared to have relatively higher level of sulfur at the thin film region. This suggests the formation of a protective sulfide layer on the metal surface, which would explain the drop in corrosion rate relative to the CO_2-only system.

DISCLAIMER

This report was prepared as an account of work sponsored by an agency of the United States Government. Neither the United States Government nor any agency thereof, nor any of their employees, makes any warranty, express or implied, or assumes any legal liability or responsibility for the accuracy, completeness, or usefulness of any information, apparatus, product, or process disclosed, or represents that its use would not infringe privately owned rights. Reference herein to any specific commercial product, process, or service by trade name, trademark, manufacturer, or otherwise does not necessarily constitute or imply its endorsement, recommendation, or favoring by the United States Government or any agency thereof. The views and opinions of authors expressed herein do not necessarily state or reflect those of the United States Government or any agency thereof.

ACKNOWLEDGMENTS

The authors would like to acknowledge OLI Systems for providing access to their modeling software. Further thanks are given to Dr. Andre Anderko for his assistance in modeling the solution speciation and corrosion rates.

REFERENCES

1. K. Videm, J. Karekval, “Corrosion of Carbon Steel in Carbon Dioxide-Saturated Solutions Containing Small Amounts of Hydrogen Sulfide.” *Corrosion* **51**, p. 260-269 (1995).
2. NACE International, “Wet Gas Internal Corrosion Direct Assessment Methodology for Pipelines.” *NACE SP0110* (2010).
3. S. Smith, “Discussion of the History and Relevance of the CO_2/H2S Ratio.” *NACE CORROSION 2011*, Paper No. 11065 (2011).
4. J. Kvarekval, R. Nyborg, M. Seiersten, “Corrosion product films on carbon steel in semi-sour CO_2/H_2S environments.” *NACE CORROSION 2002*, Paper No. 02296 (2002).
5. K. Lee, S. Nesic, “The Effect of Trace Amount of H_2S on CO_2 Corrosion Investigated by Using the EIS Technique.” *NACE CORROSION 2005*, Paper No. 05630 (2005).
6. M. Singer, B. Brown, A. Camacho, S. Nesic, “Combined Effect of CO_2, H_2S and Acetic Acid on Bottom of the Line Corrosion.” *NACE CORROSION 2007*, Paper No. 07661 (2007).
7. E. Abelev, J. Sellberg, T. A. Ramanarayanan, S. L. Bernasek, “Effect of H_2S on Fe corrosion in CO_2-saturated brine.” *J Mater Sci* **44**, p. 6167-6181 (2009).

©2016 by NACE International.
Requests for permission to publish this manuscript in any form, in part or in whole, must be in writing to
NACE International, Publications Division, 15835 Park Ten Place, Houston, Texas 77084.
The material presented and the views expressed in this paper are solely those of the author(s) and are not necessarily endorsed by the Association.

8. Y. Choi, S. Nesic, S. Ling, "Effect of H_2S on the CO_2 corrosion of carbon steel in acidic solutions." *Electrochimica Acta* **56**, p. 1752-1760 (2011).
9. J. Karekval, R. Nyborg, "Formation of multilayer iron sulfide films during high temperature CO_2/H_2S corrosion of carbon steel." *NACE CORROSION 2003*, Paper No. 03339 (2003).
10. C. Ren, D. Lio, Z. Bai, T. Li, "Corrosion behavior of oil tube steel in simulant solution with hydrogen sulfide and carbon dioxide." *Materials Chemistry and Physics* **93**, p. 305-309 (2005).
11. F. Pessu, R. Barker, A. Neville, "Early stages of pitting corrosion of UNS K013014 carbon steel in sour corrosion environments: The influence of CO_2, H_2S and temperature." *NACE CORROSION 2015*, Paper No. 5583 (2015)
12. Z. Liu, X. Wang, R. Liu, C. Du, X. Li, "Electrochemical and Sulfide Stress Corrosion Cracking Behavior of Tubing Steels in a H_2S/CO_2 Annular Environment." *Journal of Materials and Engineering Performance* **23**, p. 1279-1287 (2014).
13. ISO, ANSI, NACE International, "Petroleum and natural gas industries – Materials for use in H_2S-containing environments in oil and gas production." *ANSI/NACE MR0175/ISO 1516-1*, 2009.
14. M. Ziomek-Moroz, "Environmentally Assisted Cracking of Drill Pipes in Deep Drilling Oil and Natural Gas Wells." *Journal of Materials Engineering and Performance* **21**, p. 1061-1069 (2011).
15. K. Rozman, "Corrosion and fatigue of oil well drilling steels." Oregon State University, Master's Thesis (2011).
16. R. Feng, J. Beck, S. Lvov, M. Ziomek-Moroz, "Effects of Hydrogen Sulfide on the Corrosion Behavior of High Strength Steel in Alkaline Solutions." *ECS Transactions* **61**, p. 97-114 (2014).
17. R. Robie, B. Hemingway, J. Fisher, "Thermodynamic properties of minerals and related substances at 298.15°K and 1 bar (105 Pascals) pressure and higher temperatures." *Geol. Surv. Bull.*, No. 1452 (1978).
18. I. Zaytzev, Ed., *Properties of Aqueous Solutions of Electrolytes*. Boca Raton: CRC press Inc. (1992).
19. ASTM International, "Standard Practice for Preparing, Cleaning, and Evaluating Corrosion Test Specimens." *ASTM G1-03* (2010)
20. A. Anderko, P. McKenzie, R. Young, "Computation of Rates of General Corrosion Using Electrochemical and Thermodynamic Models." *Corrosion* **57**, p. 202-213 (2001).
21. A. Anderko, R. Young, "Simulation of CO2/H2S Corrosion Using Thermodynamic and Electrochemical Models." *NACE CORROSION 1999*, Paper No. 99031 (1999).
22. P. Sarin, V. Snoeyink, J. Bebee, W. Kriven, J. Clement, "Physico-chemical characteristics of corrosion scales in old iron pipes." *Water Res.* **35**, p. 2961–2969 (2001).

©2016 by NACE International.
Requests for permission to publish this manuscript in any form, in part or in whole, must be in writing to
NACE International, Publications Division, 15835 Park Ten Place, Houston, Texas 77084.
The material presented and the views expressed in this paper are solely those of the author(s) and are not necessarily endorsed by the Association.